How to cite: *Angew. Chem. Int. Ed.* **2020**, *59*, 18201 – 18207
International Edition: doi.org/10.1002/anie.202007241
German Edition: doi.org/10.1002/ange.202007241

Bonding Analysis

Beryllium Atom Mediated Dinitrogen Activation via Coupling with Carbon Monoxide

Guohai Deng[+], Sudip Pan[+], Guanjun Wang, Lili Zhao, Mingfei Zhou, and Gernot Frenking**

Abstract: *The reactions of laser-ablated beryllium atoms with dinitrogen and carbon monoxide mixtures form the end-on bonded NNBeCO and side-on bonded (η^2-N_2)BeCO isomers in solid argon, which are predicted by quantum chemical calculations to be almost isoenergetic. The end-on bonded complex has a triplet ground state while the side-on bonded isomer has a singlet electronic ground state. The complexes rearrange to the energetically lowest lying NBeNCO isomer upon visible light excitation, which is characterized to be an isocyanate complex of a nitrene derivative with a triplet electronic ground state. A bonding analysis using a charge- and energy decomposition procedure reveals that the electronic reference state of Be in the NNBeCO isomers has an $2s^0 2p^2$ excited configuration and that the metal-ligand bonds can be described in terms of $N_2 \rightarrow Be \leftarrow CO$ σ donation and concomitant $N_2 \leftarrow Be \rightarrow CO$ π backdonation. The results demonstrate that the activation of N_2 with the N–N bond being completely cleaved can be achieved via coupling with carbon monoxide mediated by a main group atom.*

Dinitrogen is the most abundant but highly inert molecule in Earth's atmosphere. Its activation and functionalization to valuable nitrogen-containing compounds are highly desirable but very challenging. Both the industrial Haber-Bosch process and natural nitrogenase enzymes use transition metal centers to catalyze the dinitrogen transformation processes.[1,2] Coordination of dinitrogen to the transition metal centers is proposed to be the initial step of the complex sequential chemical activation of dinitrogen.[3] Transition metals weaken the strong triple bond of dinitrogen via synergistically accepting electron density from N_2 (σ donation) and back donating electrons from their d orbitals into the antibonding π orbitals of N_2 (π back donation),[4] which are crucial for further N–N bond cleavage or functionalization with the formation of chemical bonds such as N–H or N–C.[3] A number of transition metal as well as lanthanide and actinide metal complexes have been found with N_2 ligands in various coordination modes that can facilitate catalytic or stoichiometric transformations of the N_2 unit.[5–7]

In contrast to transition metals with valence d orbitals, main group elements are reluctant to form stable complexes due to the lack of empty σ symmetry and filled π symmetry orbitals for bonding with dinitrogen. Accordingly, very few dinitrogen complexes of main group elements have been reported, most of which are not stable at ambient conditions and can only be detected in low-temperature noble gas matrices or in the gas phase.[8–13] In these complexes, the dinitrogen ligands are predominately end-on bonded with limited level of activation due to lack of strong π back donation, which prevents its propensity to be further functionalized. Only the reactive borylenes were reported to bind N_2 to form stable dinitrogen adducts and reductive coupling of two hypovalent-boron-bound N_2 units, which can be further protonated.[14] Recently, we found that the alkaline earth metal beryllium is able to form covalently side-on bonded dinitrogen complexes with drastically weakened N–N bond,[15] thus making it susceptible to dissociation. Here we report a joint matrix-isolation infrared spectroscopic and theoretical study on dinitrogen coordination and activation via coupling with carbon monoxide mediated by beryllium atoms in forming isocyanate complex with the N-N triple bond being completely cleaved.

Matrix isolated beryllium containing species were generated by codeposition of laser ablated beryllium atoms with CO and N_2 mixtures in excess argon at 4 K and investigated using Fourier transformed infrared absorption spectroscopy.[16] Augmented by the isotopic substitution technique, infrared absorption spectroscopy is a very powerful method for the structural characterization of new species isolated in matrices.[17] The experiments were performed using relatively low laser energy to avoid the formation of multinuclear species, which were reported previously to be the major products from the reactions of laser-ablated beryllium atoms with CO or N_2 in solid argon employing relatively high laser energy.[8a,18] Figure 1 shows the spectra in the C-O and N-N stretching frequency region from an experiment using a 0.5 %

[*] G. Deng,[+] G. Wang, M. Zhou
Collaborative Innovation Center of Chemistry for Energy Materials, Department of Chemistry, Shanghai Key Laboratory of Molecular Catalysts and Innovative Materials, Fudan University
Shanghai 200438 (China)
E-mail: mfzhou@fudan.edu.cn
S. Pan,[+] L. Zhao, G. Frenking
Institute of Advanced Synthesis, School of Chemistry and Molecular Engineering, Jiangsu National Synergetic Innovation Center for Advanced Materials, Nanjing Tech University
Nanjing 211816 (China)
S. Pan,[+] G. Frenking
Fachbereich Chemie, Philipps-Universität Marburg
Hans-Meerwein-Strasse 4, 35043 Marburg (Germany)
E-mail: frenking@chemie.uni-marburg.de
[+] These authors contributed equally to this work.
Supporting information and the ORCID identification number(s) for the author(s) of this article can be found under: https://doi.org/10.1002/anie.202007241.

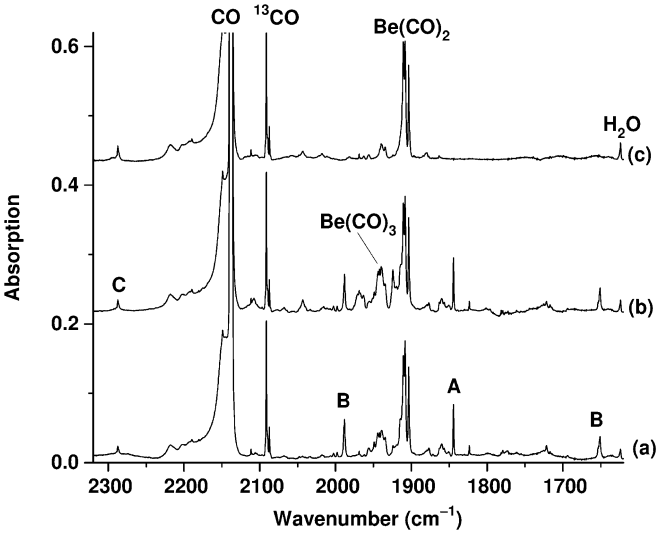

Figure 1. Infrared spectra in the 2320–1620 cm^{-1} region from co-deposition of laser-ablated beryllium atoms with 0.5% CO + 0.5% N_2 in argon. a) 1 h of sample deposition at 4 K, b) after annealing to 15 K, and c) after 15 min of visible light (440 ± 20 nm) irradiation. **A**: NNBeCO; **B**: (η^2-N_2)BeCO; **C**: NBeNCO.

N_2/0.5% CO/Ar sample (on the basis of volume). In addition to the beryllium carbonyl absorptions[18] (dominated by the $Be(CO)_2$ absorptions at 1908.3/1903.5 cm^{-1} for the antisymmetric CO stretching mode; the antisymmetric Be-C stretching mode at 1140.8 cm^{-1} is not shown in Figure 1; the tricarbonyl $Be(CO)_3$ absorption centered at 1939.4 cm^{-1} is also observed to increase on annealing), three groups of new product absorptions labeled as **A**–**C** in Figure 1 were observed after sample deposition at 4 K (Spectrum a). These absorptions were only produced in the experiments when both the N_2 and CO samples were employed. Homoleptic beryllium dinitrogen complexes were barely observed.[8a,15] Both group **A** and **B** absorptions slightly decreased on sample annealing (Spectrum b). Group **B** absorptions decreased, while group **A** absorptions increased under 617 nm light irradiation. Both were completely destroyed when the sample was subjected to 15 min of visible light (440 ± 20 nm) irradiation (Spectrum c), during which the group **C** absorption increased. Several broad bands are observed to increase on annealing. These bands are weak in the experiments using low concentration of CO. The broad band centered at 1860 cm^{-1} shows similar isotopic shifts as the 1844.5 cm^{-1} band of species **A**. It is attributed to a weakly CO or N_2 bound complex of **A**. The broad band centered at 1968 cm^{-1} is mainly a carbonyl stretching mode but shows small N-15 isotopic shift. It is due to a highly coordinated complex involving both CO and N_2 ligands. Experiments were repeated using the isotopic-labeled mixture samples including $^{15}N_2$, ^{13}CO and $C^{18}O$. The infrared spectra in selected regions with different isotopic-substituted samples are shown in Figures S1–S4, which allow the unambiguous identification of these product absorptions through isotopic shifts and splittings. The band positions of the product species are summarized in Table 1.

Species **A** with absorptions at 1844.5 and 1167.9 cm^{-1} are assigned to the NNBeCO complex with both the CO and N_2 ligands being end-on bonded. The 1844.5 cm^{-1} absorption shifted to 1799.0, 1830.3 and 1831.4 cm^{-1} with the $^{15}N_2$/CO, N_2/^{13}CO and N_2/$C^{18}O$ samples, respectively, implying that this is largely a N-N stretching mode. Only the pure isotopic counterparts were observed in the experiments using the mixed $^{12}CO + {}^{13}CO/N_2$, $C^{16}O + C^{18}O/N_2$ and $^{14}N_2 + {}^{15}N_2$/CO

Table 1: Observed infrared absorptions (cm^{-1}) of the three BeN_2CO isomers in solid argon and computed values at the CCSD(T)-Full/aug-cc-pVTZ level.

		Experimental					
	$^{12}C^{16}O/^{14}N_2$	$^{12}C^{16}O/^{15}N_2$	$\Delta(^{15}N)$	$^{13}C^{16}O/^{14}N_2$	$\Delta(^{13}C)$	$^{12}C^{18}O/^{14}N_2$	$\Delta(^{18}O)$
NNBeCO (A)	1844.5	1799.0	−45.5	1830.3	−14.2	1831.4	−13.1
	1167.9	1165.2	−2.7	1167.4	−0.5	1163.6	−4.3
(η^2-N_2)BeCO (B)	1988.3	1983.9	−4.4	1946.9	−41.4	1951.3	−37.0
	1651.1	1603.8	−47.3	1648.8	−2.3	1647.2	−3.9
	1056.1	1051.6	−4.5	1055.0	−1.1	1053.4	−2.7
NBeNCO (C)	2287.5	2274.0	−13.5	2226.3	−61.2	2273.0	−14.5
		Calculated					
NNBeCO (A)	2078.2 (1974.4)[a] *43*[b]						
	1928.3 (1840.4)[a] *4027*[b]	1887.5	−40.8	1901.8	−26.5	1904.2	−24.1
	1180.6 (1090.2)[a] *396*[b]	1178.1	−2.5	1180.4	−0.2	1176.5	−4.1
(η^2-N_2)BeCO (B)	2047.2 (2017.5)[a] *1116*[b]	2044.8	−2.4	2000.7	−46.5	2006.2	−41.0
	1681.6 (1656.0)[a] *965*[b]	1630.2	−51.4	1680.1	−1.5	1678.7	−2.9
	1100.0 (1065.3)[a] *696*[b]	1095.3	−4.7	1099.5	−0.5	1097.3	−2.7
NBeNCO (C)	2370.3 (2311.2)[a] *1690*[b]	2355.8	−14.5	2306.3	−64.0	2355.2	−15.1
	1594.0 (1560.1)[a] *145*[b]						
	1169.1 (1129.2)[a] *188*[b]						

[a] Corrected by anharmonic contribution calculated at M06-2X-D3/aug-cc-pVTZ. [b] Infrared intensity of the anharmonic vibrations in km mol^{-1}.

samples (Figure S1, spectra b, c, and e), confirming that only one CO and one N_2 ligands are involved in this mode. A quartet at 1844.5, 1824.4, 1822.3 and 1799.0 cm^{-1} with approximately 1:1:1:1 relative intensities was produced when a $^{14}N_2 + {}^{14}N^{15}N + {}^{15}N_2$ (1:2:1)/CO sample was used (Figure S1, spectrum f). This quartet feature implies that the two nitrogen atoms are inequivalent. The 1167.9 cm^{-1} absorption is due to the C-Be-N stretching mode (Figure S3).

Three absorptions were observed for species **B,** which is assigned to the (η^2-N_2)BeCO isomer involving an end-on bonded carbonyl ligand and a side-on bonded N_2 ligand. The 1988.3 cm^{-1} band shows quite small ^{15}N isotopic shift (−4.4 cm^{-1}) but quite large ^{13}C (−41.4 cm^{-1}) and ^{18}O (−37.0 cm^{-1}) isotopic shifts (Table 1), and thus, is assigned to the carbonyl stretching vibration. The doublet isotopic structures in the mixed $^{12}CO + {}^{13}CO/N_2$ and $C^{16}O + C^{18}O/N_2$ experiments (Figure S1, spectra b and c) confirm that only one CO fragment is involved in this mode. The 1651.1 cm^{-1} absorption is mainly a N-N stretching vibration with quite large ^{15}N shift (−47.3 cm^{-1}) and very small ^{13}C (−2.3 cm^{-1}) and ^{18}O (−3.9 cm^{-1}) shifts (Table 1). The isotopic shifts and the splittings in the mixed $N_2 + {}^{15}N_2/CO$ and $N_2 + {}^{14}N^{15}N + {}^{15}N_2/CO$ experiments (Figure S2) indicate that this absorption is mainly originated from a side-on bonded N_2 ligand with equivalent nitrogen atoms.

Only one band at 2287.5 cm^{-1} was observed for species **C**. This absorption increased under visible light (440 ± 20 nm) irradiation at the expense of the group **A** and **B** absorptions (Figure S5), suggesting that absorber **C** is a third structural isomer with chemical formula of BeN_2CO. The band position and isotopic shifts (Table 1) are appropriate for an antisymmetric NCO stretching vibration.[19,20] The doublet isotopic structures observed in the mixed $^{12}CO + {}^{13}CO/N_2$, $C^{16}O + C^{18}O/N_2$, $^{14}N_2 + {}^{15}N_2/CO$ as well as $N_2 + {}^{14}N^{15}N + {}^{15}N_2/CO$ experiments (Figure S4) clearly show that only one NCO subunit is involved in this mode. Accordingly, species **C** is attributed to NBeNCO, an isocyanate complex of beryllium nitride. The band position is about 364 cm^{-1} blue-shifted from that of free NCO in solid argon,[21] and is slightly higher than those of the isocyanate species previously reported in solid noble gas matrices and on metal catalyst surfaces, which were observed in the range of 2160–2270 cm^{-1} region.[19,20] The band of NBeNCO is present directly after sample deposition. It does not increase but slightly sharpens on annealing. The observation of **C** directly after sample deposition suggests that it can be formed during the sample deposition process initiated by the irradiation from the ablated plume.

We calculated the geometries and vibrational frequencies of the BeN_2CO isomers in the electronic singlet and triplet states at the CCSD(T)-Full/aug-cc-pVTZ level of theory. The relative energies of the isomers were computed with larger basis sets at CCSD(T)-Full/aug-cc-pVQZ using the CCSD-(T)-Full/aug-cc-pVTZ optimized geometries. Details of the calculations are given in the Supporting Information. Figure 2 shows the theoretically predicted equilibrium structures **A**–**C** and the calculated bond lengths and bond angles, while the energetically high-lying isomers **D**–**T** are shown in Figure S6. The global energy minimum is the linear structure NBeNCO (**C**) in the triplet ($^3\Sigma$) state. The side-on bonded (η^2-N_2)BeCO isomer **B** in the singlet ($^1A_1$) state is 4.7 kcal mol^{-1} higher in energy than **C**. The linear species NNBeCO (**A**) in the electronic triplet ($^3\Sigma$) state is energetically only slightly (0.7 kcal mol^{-1}) higher lying than **B**, and lies 5.4 kcal mol^{-1} above the most stable form **C**. The other isomers **D**–**T** are clearly higher in energy than **A**–**C** (Figure S6). The formation of the energetically closest two isomers, ONBeNC (**D**) and ONBeCN (**E**) in the electronic triplet state ($^3\Sigma$), which are 7.8 and 9.5 kcal mol^{-1} higher in energy than **C**, involves breaking both the N–N and C–O bonds. The two next higher-lying isomers NNBeCO (**F**) in the electronic singlet ($^1\Sigma$) state and the side-on bonded (η^2-N_2)BeCO (**G**) in the triplet ($^3A_2$) state lie 11.8 and 13.2 kcal mol^{-1} above **C**. The isomer OBeCNN (**Q**, $^3\Sigma$) is 64.4 kcal mol^{-1} higher in energy than **C**, which makes it unlikely to be formed during the reaction. For the end-on bonded isomers holds that the triplet state is always favored over the singlet state, whereas for the side-on bonded species exhibit the opposite stability order.

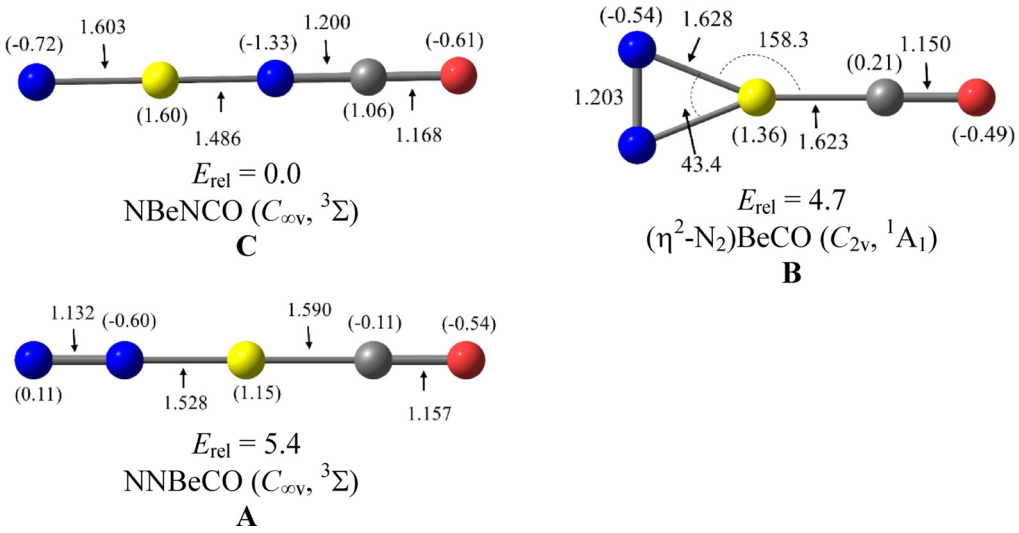

Figure 2. The geometries of different isomers of BeN_2CO complex at the CCSD(T)-Full/aug-cc-pVTZ level. Bond distances are in Å and bond angles are in degree. The atomic partial charges calculated by the NBO method are given in parentheses. The relative energies in kcal mol^{-1} are at the CCSD(T)-Full/aug-cc-pVQZ//CCSD(T)-Full/aug-cc-pVTZ level.

Table 1 shows the calculated harmonic vibrational frequencies and isotopic shifts of the three energetically lowest lying isomer **A**–**C**. The first column gives in parentheses the theoretical values, which are corrected by anharmonic contributions that are calculated at the

M06-2X-D3/aug-cc-pVTZ level. Anharmonic vibrational frequencies at CCSD(T)-Full/aug-cc-pVTZ are not available. The agreement of the calculated anharmonic vibrations and the isotope shifts with the experimental values is very good. Somewhat larger deviations are found for the linear structure **A**, which may be caused by the very shallow bending potential. Calculations with smaller basis sets give a bent equilibrium structure of **A**. A geometry optimization of **A** with an enforced bending angle NN-Be-CO = 120° at the CCSD(T)-Full/aug-cc-pVTZ level gives a structure, which is only 0.1 kcal mol^{-1} higher in energy than the linear equilibrium form. The very soft bending potential is likely the reason for the different values for **A** particularly for the isotope shifts. The highest lying mode of **A** and the two lowest lying frequencies of **C** shown on Table 1 have a very small IR intensity, which explains why these signals are not observed in experiment. The possibility of the existence of two somehow energetically competitive isomers, **D** and **E**, is excluded from the inspection of the related IR frequencies and isotopic shifts given in Table S1. The comparison of calculated vibrational frequencies and isotope shifts with the experimental results leaves no doubt about the assignment of the spectra to the three structures **A**–**C** shown in Figure 2.

Experimentally **C** is formed under visible light irradiation of species **A** and **B**. The possible isomeric pathways involve the sequence **A**→**G**→**C** and **B**→**G**→**C** where the second pathway requires a change of the spin state. Figure S7 shows the first pathway where the step **A**→**G** involves an activation energy barrier of 25.3 kcal mol^{-1} and the second step **G**→**C** requires to cross a high barrier of 134.5 kcal mol^{-1}. The TDDFT calculation on **B** at the M06-2X/aug-cc-pVTZ level shows that the vertical $^1A_1 \rightarrow {}^3A_2$ transition requires excitation energy of 17.6 kcal mol^{-1} energy (Figure S8). The vertically excited $^3A_2$ state would then rearrange to **G**, before finally converting into the most stable isomer **C**. The simulated UV/vis spectra for **A** and **B** are displayed in Figure S9, which show strong absorption bands at 339 and 318 nm.

We analyzed the electronic structures of **A**–**C** with a variety of methods in order to understand the bonding situation in the three molecules. Figure 3 shows the shape of the highest lying occupied MOs, which give a first insight into the chemical bonds. The degenerate singly occupied MOs (SOMO) of the triplet species NNBeCO reveals that the unpaired electrons of **A** occupy the p(π) AOs of Be and the antibonding π* MOs of the N_2 and CO ligands. The shape of the HOMO of singlet (η^2-N_2)BeCO shows that a similar situation is found for the two highest lying bonding electrons of **B**. This means that the electronic reference states of Be

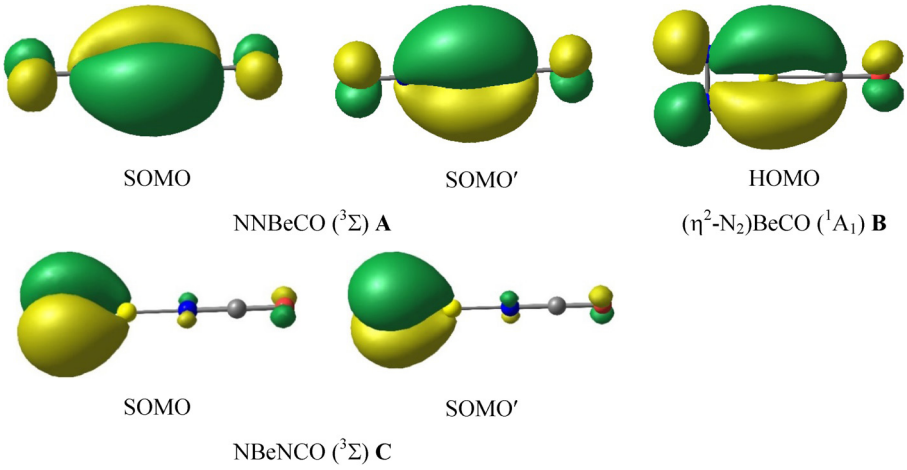

Figure 3. Shape of the energetically highest lying occupied MOs of **A**–**C**.

Table 2: EDA-NOCV results of the complexes **A** and **B** at the M06-2X/TZ2P//CCSD(T)-Full/aug-cc-pVTZ level taking beryllium atom in the electronic reference configuration and singlet (S) or triplet (T) electronic state and the ligands in the singlet state as interacting fragments. Energy values are in kcal mol^{-1}.

Energies	Orbital interaction	A [Be] (T, $2s^02p^2$) + [NN···CO] (S)	B [Be] (S, $2s^02p^2$) + [(η^2-N_2)···CO] (S)
ΔE_{int}		−180.3	−200.1
ΔE_{Pauli}		65.6	149.9
$\Delta E_{Metahybrid}$		16.6	12.0
ΔE_{elstat}[a]		−63.4 (24.2%)	−84.3 (23.3%)
ΔE_{orb}[a]		−199.1 (75.8%)	−277.8 (76.7%)
$\Delta E_{orb(1)}$[b]	[Be(p_π)]→[NN···CO] π backdonation[c]	−111.4 (56.0%)[c]	−192.8 (69.4%)
$\Delta E_{orb(2)}$[b]	[Be(p_σ)]←[NN···CO] (+,−) σ donation	−47.8 (24.0%)	−43.9 (15.8%)
$\Delta E_{orb(3)}$[b]	[Be(s)]←[NN···CO] (+,+) σ donation	−19.9 (10.0%)	−17.7 (6.4%)
$\Delta E_{orb(4)}$[b]	[Be($p_\perp$)]←[(η^2-N_2)···CO] $\pi_\perp$ donation		−9.7 (3.5%)
ΔE_{rest}[b]		−20.0 (10.0%)	−13.7 (4.9%)
ΔE_{prep}(Be)	Be($2s^2$) → Be(^{3}P($2s^02p^2$))	155.4	
	Be($2s^2$) → Be(^{1}D($2s^02p^2$))		171.7
ΔE_{prep}(NN···CO)	N_2/CO → NN···CO	6.0	21.3

[a] The values in parentheses give the percentage contribution to the total attractive interactions $\Delta E_{elstat} + \Delta E_{orb}$. [b] The values in parentheses give the percentage contribution to the total orbital interactions ΔE_{orb}. [c] Two components.

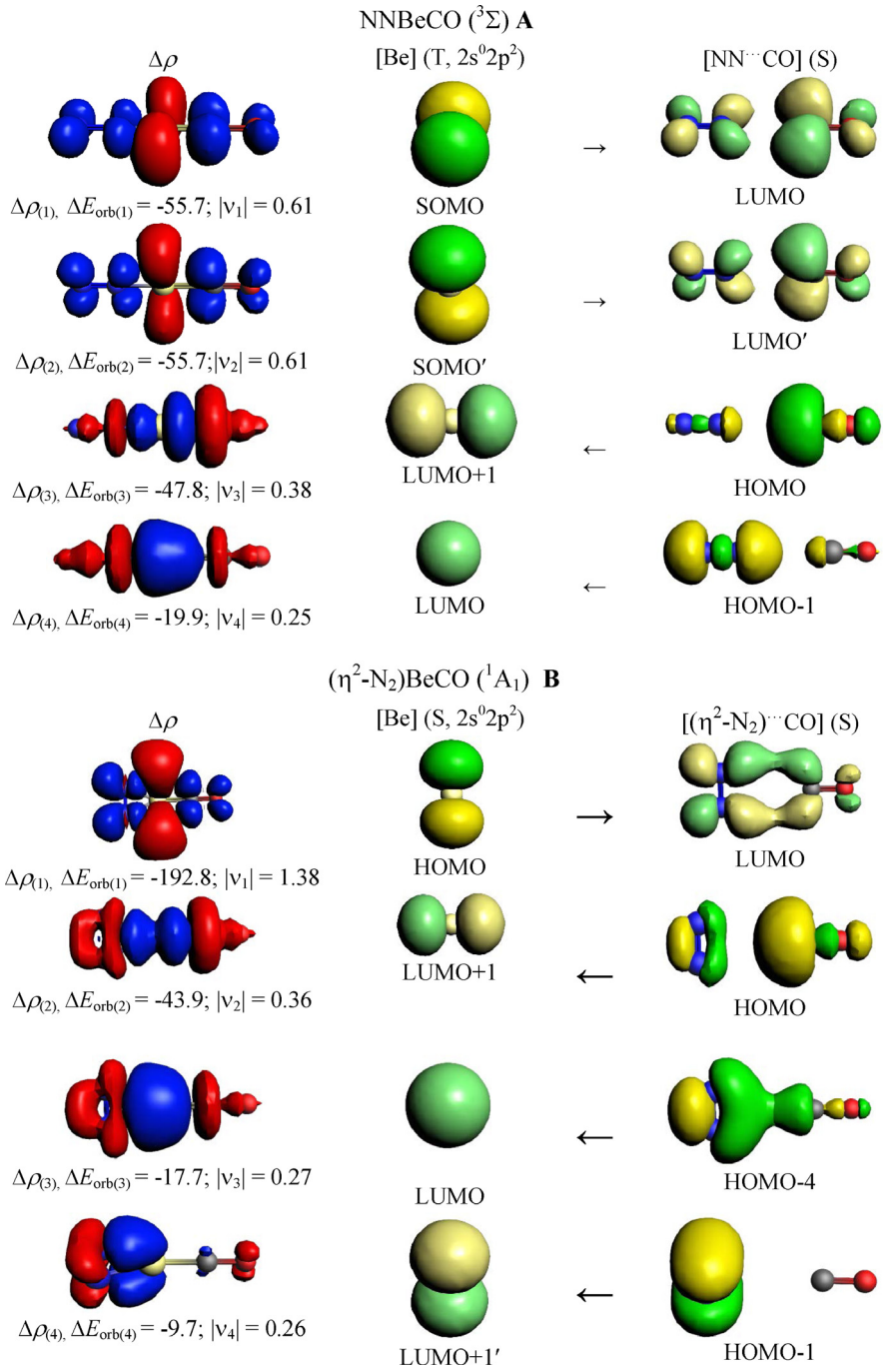

Figure 4. Shape of the deformation densities, $\Delta\rho_{(1)\text{-}(4)}$ of **A** and **B** corresponding to $\Delta E_{orb(1)}$–$\Delta E_{orb(4)}$ and the associated fragment orbitals at the M06-2X/TZ2P//CCSD(T)-Full/aug-cc-pVTZ level. Isosurface values are 0.001 au. The eigenvalues $|\nu_n|$ give the size of the charge migration in e. The direction of the charge flow of the deformation densities is red→blue.

atom in **A** and **B** are the excited $^3P(2s^02p^2)$ and $^1D(2s^02p^2)$ states, respectively, where the valence electrons are in the 2p AOs. Table 2 gives the numerical results of the EDA-NOCV (energy decomposition analysis with natural orbitals for chemical valence)[22] calculations using Be atom in the ^3P and ^1D reference state and the N_2···CO ligands as interacting fragments. The choice of neutral fragments, which are the final product of the bond cleavage, means that the calculated interactions include all intra- and interfragment alterations of the electronic structure. The EDA-NOCV method has been shown to give deep insight into the nature of interatomic interactions.[23]

The data in Table 2 show that the orbital mixing ΔE_{orb} provides three quarter of the total attraction between the fragments whereas electrostatic interaction contributes only one quarter. The largest stabilization of the orbital interactions in **A** and **B** comes from the π backdonation of the occupied $2p_\pi$ AO of Be to the π* MOs of the ligands. The donation of the σ donor orbitals due to the in-phase (+,+) and out-of-phase (+,−) combination of the ligand orbitals are much weaker. There is also a further small contribution in **B** from the $\pi_\perp$ donation of the ligands into the vacant $p_\perp$ AO of Be. The pairwise orbital interactions are nicely visualized and identified with the help of the associated deformation densities $\Delta\rho$ shown in Figure 4. The shape and the size of the charge flow, which is given by the eigenvalues $|\nu_n|$ of $\Delta\rho_{(n)}$, provide detailed insight into the change of the electronic structure of the fragments through the bonding interactions. The net charge flow of donation and backdonation between beryllium and the ligands given by the four dominant interactions suggests that Be has a positive partial charge of +0.59 in **A** and +0.46 in **B**. These positive charges for beryllium are much smaller than the values suggested by the NBO method given in Figure 2, which are +1.15 for **A** and +1.36 for **B**. However, the NBO method does not consider the 2p AOs of beryllium as valence orbitals but rather as so-called Rydberg orbitals, which are differentially weighted in the NBO algorithm. The NBO method considers only those AOs as genuine valence orbitals, which are occupied in the electronic ground state of the respective atoms.[24] This has been criticized in the past[25] and it was recently shown to lead to an unrealistic description of the bonding situation.[26] It is well known that the electronic reference state of an atom in a molecule may be an excited state.

The bonding situation in the NNBeCO isomers **A** and **B** can thus be described in terms of σ donation of the ligands N_2 and CO into the vacant 2s and $2p_\sigma$ AOs of Be in the $2s^02p^2$ excited configuration N_2→Be←CO and concomitant π back-

donation of the $2p_\pi$ electrons of Be into the π* MOs of the ligands $N_2 \leftarrow Be \rightarrow CO$, which provides the largest contribution to the orbital interactions. Table 2 also shows that the intrinsic interaction energy ΔE_{int} between the promoted beryllium atom and the N_2 and CO ligands with frozen geometries is nearly 20 kcal mol^{-1} larger in isomer **B** than in **A**. This is due to the fact that the electronic and geometric preparation energies of the fragments in **B** are much higher than in **A**.

The shape of the degenerate SOMO of the triplet species NBeNCO (**C**) shows that the unpaired electrons are in the orthogonal bonding π MOs of the NBe moiety, which are strongly polarized towards the terminal nitrogen atom (Figure 3). NBeNCO is thus a triplet state nitrene derivative.[27] This finding and the calculated charge distribution given in Figure 2 suggest that the bonding situation in **C** is best discussed using NBe^+ cation and NCO^- anion as interacting fragments. The EDA-NOCV results for **C** using NBe^+ and NCO^- as fragments give a straightforward picture of the bonds (Table S2, Supporting Information). Two third of the bonding comes from the Coulombic attraction and one third from the orbital (covalent) interaction. The largest stabilization caused by orbital interactions is due to the π donation of the degenerate π bonding MOs of the isocyanate anion $NBe^+ \leftarrow\!\!\rightarrow NCO^-$ followed by σ donation $NBe^+ \leftarrow NCO^-$. Figure S10 of Supporting Information shows the associated charge flow of the σ and π donation and the orbital of the fragments. As expected, the π backdonation $NBe^+ \rightarrow NCO^-$ is rather weak.

In summary, we report the reactions of laser-ablated beryllium atoms with dinitrogen and carbon monoxide mixtures forming the end-on bonded NNBeCO **A** and side-on bonded (η^2-N_2)BeCO **B** isomers in solid argon, which are predicted by quantum chemical calculations to be almost isoenergetic. The end-on bonded complex has a triplet ground state while the side-on bonded isomer has a singlet electronic ground state. The complexes rearrange to the energetically lowest lying NBeNCO isomer upon visible light excitation, which is characterized to be an isocyanate complex of a nitrene derivative with a triplet electronic ground state. A bonding analysis using a sophisticated charge- and energy decomposition procedure reveals that the electronic reference state of Be in the NNBeCO isomers **A** and **B** has an $2s^0 2p^2$ excited configuration and that the metal-ligand bonds can be described in terms of $N_2 \rightarrow Be \leftarrow CO$ σ donation and concomitant $N_2 \leftarrow Be \rightarrow CO$ π backdonation.

Acknowledgements

The experimental work was supported by the National Natural Science Foundation of China (grant numbers 21688102). L.Z. and G.F. acknowledge financial support from Nanjing Tech University (grant numbers 39837123, 39837132) and SICAM Fellowship from Jiangsu National Synergetic Innovation Center for Advanced Materials, Natural Science Foundation of Jiangsu Province for Youth (grant number BK20170964), National Natural Science Foundation of China (grant numbers 21703099, 21993044). S.P. thanks Deutsche Forschungsgemeinschaft for a postdoctoral fellowship. Open access funding enabled and organized by Projekt DEAL.

Conflict of interest

The authors declare no conflict of interest.

Keywords: beryllium · bonding analysis · dinitrogen activation · infrared photodissociation spectroscopy · matrix isolation

[1] R. Schlögl, *Ammonia Synthesis in Handbook of Homogeneous Catalysis* (Eds.: G. Ertl, H. Knözinger, F. Schüth, J. Weitkamp), Wiley, Hoboken, **2008**.

[2] a) B. K. Burgess, D. J. Lowe, *Chem. Rev.* **1996**, *96*, 2983 – 3012; b) B. M. Hoffman, D. Lukoyanov, Z. Y. Yang, D. R. Dean, L. C. Seefeldt, *Chem. Rev.* **2014**, *114*, 4041 – 4062.

[3] a) R. R. Schrock, *Acc. Chem. Res.* **2005**, *38*, 955 – 962; b) N. Hazari, *Chem. Soc. Rev.* **2010**, *39*, 4044 – 4056; c) K. C. MacLeod, P. L. Holland, *Nat. Chem.* **2013**, *5*, 559 – 565; d) H. Tanaka, Y. Nishibayashi, K. Yoshizawa, *Acc. Chem. Res.* **2016**, *49*, 987 – 995; e) R. J. Burford, A. Yeo, M. D. Fryzuk, *Coord. Chem. Rev.* **2017**, *334*, 84 – 99.

[4] a) M. J. S. Dewar, *Bull. Soc. Chim. Fr.* **1951**, *18*, C79; b) J. Chatt, L. A. Duncanson, *J. Chem. Soc.* **1953**, 2929; c) N. Fröhlich, G. Frenking, *Chem. Rev.* **2000**, *100*, 717.

[5] a) M. Hidai, Y. Mizobe, *Chem. Rev.* **1995**, *95*, 1115 – 1133; b) H. J. Himmel, M. Reiher, *Angew. Chem. Int. Ed.* **2006**, *45*, 6264 – 6288; *Angew. Chem.* **2006**, *118*, 6412 – 6437; c) J. G. Andino, S. Mazumder, K. Pal, K. G. Caulton, *Angew. Chem. Int. Ed.* **2013**, *52*, 4726 – 4732; *Angew. Chem.* **2013**, *125*, 4824 – 4831; d) C. Geng, J. Li, T. Weiske, H. Schwarz, *Proc. Natl. Acad. Sci. USA* **2018**, *115*, 11680 – 11687.

[6] a) B. A. MacKay, M. D. Fryzuk, *Chem. Rev.* **2004**, *104*, 385 – 401; b) R. J. Burford, M. D. Fryzuk, *Nat. Rev. Chem.* **2017**, *1*, 0026.

[7] a) P. Roussel, P. Scott, *J. Am. Chem. Soc.* **1998**, *120*, 1070 – 1071; b) M. F. Zhou, X. Jin, Y. Gong, J. Li, *Angew. Chem. Int. Ed.* **2007**, *46*, 2911 – 2914; *Angew. Chem.* **2007**, *119*, 2969 – 2972; c) M. Falcone, L. Chatelain, R. Scopelliti, I. Zivkovic, M. Mazzanti, *Nature* **2017**, *547*, 332 – 335; d) E. Lu, B. E. Atkinson, A. J. Wooles, J. T. Boronski, L. R. Doyle, F. Tuna, J. D. Cryer, P. J. Cobb, I. J. Vitorica-Yrezabal, G. F. S. Whitehead, N. Kaltsoyannis, S. T. Liddle, *Nat. Chem.* **2019**, *11*, 806 – 811; e) M. Falcone, L. Barluzzi, J. Andrez, F. F. Tirani, I. Zivkovic, A. Fabrizio, C. Corminboeuf, K. Severin, M. Mazzanti, *Nat. Chem.* **2019**, *11*, 154 – 160.

[8] a) C. A. Thompson, L. Andrews, R. D. Davy, *J. Phys. Chem.* **1995**, *99*, 7913 – 7924; b) R. R. Lembke, R. F. Ferrante, W. Weltner, Jr., *J. Am. Chem. Soc.* **1977**, *99*, 416 – 423; c) G. Maier, H. P. Reisenauer, J. Glatthaar, *Organometallics* **2000**, *19*, 4775 – 4783; d) M. Bahou, K. Sankaran, Y.-J. Wu, Y.-P. Lee, D. Rayner, B. Simard, *J. Chem. Phys.* **2003**, *118*, 9710 – 9718; e) R. C. Spiker, C. Trindle, L. Andrews, *J. Am. Chem. Soc.* **1972**, *94*, 2401 – 2406; f) L. Manceron, M. Hawkins, L. Andrews, *J. Phys. Chem.* **1986**, *90*, 4987 – 4993.

[9] a) G. Maier, H. P. Reisenauer, J. Henkelmann, C. Kliche, *Angew. Chem. Int. Ed. Engl.* **1988**, *27*, 295 – 296; *Angew. Chem.* **1988**, *100*, 303 – 303; b) M. Winkler, W. Sander, *J. Org. Chem.* **2006**, *71*, 6357 – 6367.

[10] a) J. Jin, G. J. Wang, M. F. Zhou, D. M. Andrada, M. Hermann, G. Frenking, *Angew. Chem. Int. Ed.* **2016**, *55*, 2078 – 2082; *Angew. Chem.* **2016**, *128*, 2118 – 2122; b) K. Edel, M. Krieg, D. Grote, H. F. Bettinger, *J. Am. Chem. Soc.* **2017**, *139*, 15151 – 15159.

[11] a) D. L. Robbins, L. R. Brock, J. S. Pilgrim, M. A. Duncan, *J. Chem. Phys.* **1995**, *102*, 1481 – 1492; b) S. H. Pullins, J. E. Reddic, M. R. France, M. A. Duncan, *J. Chem. Phys.* **1998**, *108*, 2725 – 2732; c) L. R. Brock, M. A. Duncan, *J. Phys. Chem.* **1995**, *99*, 16571 – 16575.
[12] a) H. J. Himmel, N. Hebben, *Chem. Eur. J.* **2005**, *11*, 4096 – 4102; b) D. Kurzbach, A. Sharma, D. Sebastiani, K. W. Klinkhammer, D. Hinderberger, *Chem. Sci.* **2011**, *2*, 473 – 479.
[13] Q. Wang, S. Pan, S. J. Lei, J. Y. Jin, G. H. Deng, G. J. Wang, L. L. Zhao, M. F. Zhou, G. Frenking, *Nat. Commun.* **2019**, *10*, 3375.
[14] a) M. A. Légaré, G. Bélanger-Chabot, R. D. Dewhurst, E. Welz, I. Krummenacher, B. Engels, H. Braunschweig, *Science* **2018**, *359*, 896 – 899; b) D. L. J. Broere, P. L. Holland, *Science* **2018**, *359*, 871; c) M. A. Légaré, M. Rang, G. Bélanger-Chabot, J. I. Schweizer, I. Krummenacher, R. Bertermann, M. Arrowsmith, M. C. Holthausen, H. Braunschweig, *Science* **2019**, *363*, 1329 – 1332.
[15] G. H. Deng, S. Pan, G. J. Wang, L. L. Zhao, M. F. Zhou, G. Frenking, *Angew. Chem. Int. Ed.* **2020**, *59*, 10603 – 10609; *Angew. Chem.* **2020**, *132*, 10690 – 10696.
[16] G. J. Wang, M. F. Zhou, *Int. Rev. Phys. Chem.* **2008**, *27*, 1 – 25.
[17] a) V. E. Bondybey, A. M. Smith, J. Argreiter, *Chem. Rev.* **1996**, *96*, 2113; b) M. F. Zhou, L. Andrews, C. W. Bauschlicher, *Chem. Rev.* **2001**, *101*, 1931 – 1961; c) Y. Gong, M. F. Zhou, L. Andrews, *Chem. Rev.* **2009**, *109*, 6765 – 6808.
[18] a) L. Andrews, T. J. Tague, Jr., G. P. Kushto, R. D. Davy, *Inorg. Chem.* **1995**, *34*, 2952 – 2961; b) W. L. Li, Q. N. Zhang, M. H. Chen, H. S. Hu, J. Li, M. F. Zhou, *Angew. Chem. Int. Ed.* **2020**, *59*, 6923 – 6928; *Angew. Chem.* **2020**, *132*, 6990 – 6995.
[19] a) J. W. Jian, Q. N. Zhang, X. Wu, M. F. Zhou, *J. Phys. Chem. A* **2017**, *121*, 7861 – 7868; b) X. F. Wang, M. F. Zhou, L. Andrews, *J. Phys. Chem. A* **2000**, *104*, 10104 – 10111; c) X. F. Wang, M. F. Zhou, L. Andrews, *J. Phys. Chem. A* **2000**, *104*, 7964 – 7973; d) X. F. Wang, L. Andrews, *J. Phys. Chem. A* **2001**, *105*, 4403 – 4409.
[20] a) M. L. Unland, *Science* **1973**, *179*, 567 – 569; b) M. L. Unland, *J. Phys. Chem.* **1973**, *77*, 1952 – 1956; c) D. I. Kondarides, T. Chafik, X. E. Verykios, *J. Catal.* **2000**, *193*, 303 – 307; d) N. Bion, J. Saussey, M. Haneda, M. Daturi, *J. Catal.* **2003**, *217*, 47 – 58.
[21] D. E. Milligan, M. E. Jacox, *J. Chem. Phys.* **1967**, *47*, 5157 – 5168.
[22] a) A. Michalak, M. Mitoraj, T. Ziegler, *J. Phys. Chem. A* **2008**, *112*, 1933; b) M. P. Mitoraj, A. Michalak, T. Ziegler, *J. Chem. Theory Comput.* **2009**, *5*, 962; c) L. Zhao, M. von Hopffgarten, D. M. Andrada, G. Frenking, *WIREs Comput. Mol. Sci.* **2018**, *8*, e1345; d) L. Zhao, M. Hermann, W. H. E. Schwarz, G. Frenking, *Nat. Rev. Chem.* **2019**, *3*, 48.
[23] a) G. Frenking, F. M. Bickelhaupt in *The Chemical Bond. Fundamental Aspects of Chemical Bonding*, (Eds.: G. Frenking, S. Shaik), Wiley-VCH, Weinheim, **2014**, pp. 121 – 158; b) G. Frenking, R. Tonner, S. Klein, N. Takagi, T. Shimizu, A. Krapp, K. K. Pandey, P. Parameswaran, *Chem. Soc. Rev.* **2014**, *43*, 5106; c) L. Zhao, M. Hermann, N. Holzmann, G. Frenking, *Coord. Chem. Rev.* **2017**, *344*, 163; d) G. Frenking, M. Hermann, D. M. Andrada, N. Holzmann, *Chem. Soc. Rev.* **2016**, *45*, 1129; e) L. Zhao, S. Pan, N. Holzmann, P. Schwerdtfeger, G. Frenking, *Chem. Rev.* **2019**, *119*, 8781.
[24] a) F. Weinhold, C. R. Landis, *Discovering Chemistry With Natural Bond Orbitals*, Wiley, Hoboken, **2012**; b) F. Weinhold, C. R. Landis, *Valency and Bonding: A Natural Bond Orbital Donor-Acceptor Perspective*, Cambridge University Press, Cambridge, **2005**.
[25] a) F. Maseras, K. Morokuma, *Chem. Phys. Lett.* **1992**, *195*, 500 – 504; b) C. A. Bayse, M. B. Hall, *J. Am. Chem. Soc.* **1999**, *121*, 1348 – 1358; c) A. Diefenbach, F. M. Bickelhaupt, G. Frenking, *J. Am. Chem. Soc.* **2000**, *122*, 6449 – 6458.
[26] C. Chi, S. Pan, L. Meng, M. Luo, L. Zhao, M. Zhou, G. Frenking, *Angew. Chem. Int. Ed.* **2019**, *58*, 1732 – 1738; *Angew. Chem.* **2019**, *131*, 1746 – 1752.
[27] C. Wentrup, *Angew. Chem. Int. Ed.* **2018**, *57*, 11508 – 11521; *Angew. Chem.* **2018**, *130*, 11680 – 11693.

Manuscript received: May 19, 2020
Accepted manuscript online: June 25, 2020
Version of record online: August 13, 2020

